

Ag-Cu nanoalloys: An electrochemical sensor for H₂O₂ detection

Muhammad Shafa^{a,1}, Iqbal Ahmad^{b,1,*}, Shahid Hussain^{c,**}, Muhammad Asif^b, Yi Pan^a, Rustem Zairov^e, Asma A. Alothman^f, Mohamed Ouladsmame^f, Zahid Ullah^g, Nabi Ullah^h, Chen Lai^d, Uzma Jabeenⁱ

^a State Key Laboratory for Mechanical Behavior of Materials, School of Materials Science and Engineering, Xi'an Jiaotong University, Xi'an 710049, China

^b Department of Chemistry, Allama Iqbal Open University, Islamabad 44000, Pakistan

^c School of Materials Science and Engineering, Jiangsu University, Zhenjiang 212013, China

^d School of Chemical Engineering and Technology, Xi'an Jiaotong University, Xi'an 710049, China

^e Aleksander Butlerov Institute of Chemistry, Kazan Federal University, 1/29 Lobachevskogo str., Kazan 420008, Russian Federation

^f Department of Chemistry, College of Science, King Saud University, Riyadh 11451, Saudi Arabia

^g Department of Environmental Science, Allama Iqbal Open University, Islamabad 44000 Pakistan

^h Department of Inorganic and Analytical Chemistry, Faculty of Chemistry, University of Lodz, Tamka 12, Lodz 90-403, Poland

ⁱ Faculty of Basic Sciences, Sardar Bahadur Khan Women's University Quetta 87300, Pakistan

ARTICLE INFO

Keywords:

Nanoalloys

H₂O₂ sensors

Cyclic voltammetry

Electrochemical impedance spectroscopy

Charge transfer resistance

ABSTRACT

Nanoalloys (Ag-Cu)-based electrochemical sensor for H₂O₂ detection has been fabricated. Pure silver (Ag) nanoparticles (NPs) and silver-copper (Ag-Cu) nanoalloys have been synthesized by using chemical reduction methodology while ratios of precursors vary as 9:1, 8:2, 7:3 and 6:4. Characterization of the prepared samples has been carried out by X-ray diffraction (XRD) which revealed the face centered cubic crystal structure of Ag NPs and Ag-Cu nanoalloys. An average crystallite size of powdered samples was calculated from XRD analysis to be 20–50 nm. Scanning electron microscopy exhibits spherical distribution of nanoparticles of the prepared alloys. A red shift was measured using UV–visible spectroscopy corresponding to the increase of copper contents in Ag-Cu nanoalloys. Cyclic voltammetric (CV) response of nanoalloys modified glassy carbon electrode was recorded in phosphate buffer of pH 7.4 in the absence and presence of H₂O₂. CV results demonstrate reduction of H₂O₂ at 0 V. Charge transfer resistance (R_{ct}) has been calculated from electrochemical impedance spectroscopy and is considered as sensing parameter in the present study. Among all the compositions, Ag-Cu (9:1) nanoalloys have shown the best sensing performance towards detection of H₂O₂ having limit of detection (LOD) and limit of quantification (LOQ) of 152 μM and 508 μM, respectively.

1. Introduction

Hydrogen peroxide (H₂O₂) is a valuable compound employed as a mediator in biological systems [1]. It plays an important role in the physiological control of hormones where it can regulate the growth of the cell including cell signaling, apoptosis and immune activation due to its reactive nature with oxygen species [2–4]. However, an excess discharge of H₂O₂ can cause cell damage [5], inflammatory disease [6], and cancer [7,8]. It also serves as an oxidant in various fields, for example food security [9], environmental monitoring [10], medical applications [11], etc., and testing and determination of H₂O₂ are of

great implication [12]. Practically, numerous methods have been developed for the detection of H₂O₂ including chromatography [13], colorimetric [14], titration [3], photoelectrochemical [15], light detection [16] and electrochemical [17,18], while titration and chromatography can't be used for the *in vitro* and *in vivo* detection of H₂O₂ [19,20]. Furthermore, light detection and chemiluminescent techniques are not convenient to detect H₂O₂ due to the variation in excitation method and the interaction of H₂O₂ with chemical compounds for fluorescence measurements [21,22]. However, electrochemical sensors possess sensitivity, specificity, good resolution with low power requirements, low cost, and linear output. These sensors are based on

* Corresponding author at: School of Chemical Engineering and Technology, Xi'an Jiaotong University, Xi'an 710049, China.

** Corresponding author.

E-mail addresses: iqbalahmadchem@gmail.com (I. Ahmad), shahid@ujs.edu.cn (S. Hussain).

¹ These authors contributed equally to this work.

electrochemically active catalysts.

Metal nanoparticles are recognized as efficient catalysts for the electrochemical monitoring of H_2O_2 due to their relatively outstanding electrical conductivity, high surface to volume ratio [23–26], and significant electrocatalytic performance [27–30], which not only favor their charge transport phenomenon but also provide large number of catalytic sites in the H_2O_2 electrochemical process [31]. The functionalization of the specific surface of Ag and Cu nanoparticles (NPs) have been exploited in bio-sensing [32–34], electronics/electro-optical devices [35,36], catalysis [37,38], sensors [39–41], textile [42] and pharmaceutical industries [43]. Due to these properties, Ag and Cu nanoparticles and its nanoalloys are used as sensors. Different nanomaterials have extensively been studied as electrochemical sensors. However, electrochemical sensing applications of Ag-Cu based nanoalloys have rarely been investigated. Furthermore, Ag and Cu NPs are good candidates to fabricate electrochemical sensors due to their low cost compared to other expensive metals like gold and platinum, etc. [44,45]. Major drawback in utilizing Cu NPs for the fabrication of sensor is oxidation that happen upon exposure to open atmosphere. To handle this problem, nanoalloys of Cu and Ag are proposed in this study that can tolerate decomposing effects.

In present work, electrochemical sensors based on Ag NPs and Ag-Cu nanoalloys have been synthesized by using chemical reduction methodology. Ag-Cu nanoalloys having different compositions (9:1, 8:2, 7:3 and 6:4) were prepared by varying the molar ratios of silver and copper by adjusting the amounts of chemical reagents. After successful growth, these nanoalloys were characterized by UV-Visible spectroscopy, XRD and SEM. Finally, electrochemical sensing properties of nanoalloys were studied by CV and EIS. Among all the samples, Ag-Cu (9:1) nanoalloy has shown the best sensing performance towards detection of H_2O_2 having LOD of $638 \mu\text{M}$ and LOQ of 2.1 mM .

2. Experimental

2.1. Materials and reagents

All chemicals used in present study were of research grade and were used without further purification. Chemicals and reagents used in the present study are silver nitrate (AgNO_3) 99.5% from Merck, copper acetate hydrate ($\text{Cu}(\text{COOCH}_3)_2 \cdot \text{H}_2\text{O}$) 98%, polyvinylpyrrolidone (PVP) MW = 40,000, sodium borohydride (NaBH_4) 98% and Nafion solution (5 wt.%) from Sigma Aldrich.

2.1.1. Synthesis of pure Ag nanoparticles

The required amount of AgNO_3 (0.85 g) was dissolved in 50 mL of distilled water to prepare 0.1 M silver nitrate solution. In a separate flask, PVP-40,000 (1.01 g) and NaBH_4 (0.4 g) were dissolved in 50 mL of distilled water and were stirred together for half an hour under inert conditions by purging Argon gas into the mixture. The AgNO_3 solution was added drop-wise to the solution of NaBH_4 and PVP, after complete

addition AgNO_3 solution the reaction mixture was stirred for 1 h more under inert atmosphere. The color of the solution became black which indicates the formation of Ag nanoparticles. After completion of reaction, the nanoparticles were separated by ultracentrifugation, washed with deionised (DI) water many times and then kept in the oven for 5 h at 80°C for drying under argon environment.

2.1.2. Synthesis of Ag-Cu nanoalloys

Ag-Cu nanoalloys of different compositions (9:1, 8:2, 7:3 and 6:4) were prepared by varying the molar ratios of silver and copper by adjusting the amounts of AgNO_3 and $\text{Cu}(\text{COOCH}_3)_2 \cdot \text{H}_2\text{O}$. Shortly, the required amounts of AgNO_3 and $\text{Cu}(\text{COOCH}_3)_2 \cdot \text{H}_2\text{O}$ were dissolved in 100 mL of distilled water. Separately, a solution of NaBH_4 and PVP-40,000 was prepared by dissolving their required amount in 100 mL of distilled water and stirred for half an hour under continuous purging of Argon gas to create inert environment. The Ag-Cu nanoalloys were prepared by dropping the AgNO_3 and $\text{Cu}(\text{COOCH}_3)_2 \cdot \text{H}_2\text{O}$ solution into the solution of NaBH_4 and PVP slowly. After complete addition, the solution was kept on stirring for 1 h. After completion of reaction, the prepared Ag-Cu nanoalloys were separated by ultracentrifugation, washed with DI water many times and then kept in the oven for 5 h at 80°C for drying under argon environment.

2.2. Characterization

UV-Visible spectra of synthesized Ag NPs and Ag-Cu nanoalloys suspended in ethanol were carried out by UV-Visible spectrophotometer (Schimadzu 1700) with a deuterium and tungsten halogen lamps as source of light and scanning wavelength ranging from 200 to 800 nm. The absorbance was scanned from 800 to 200 nm by using a quartz cuvette. The PANalytical X'Pert PRO 3040/60 X-Ray diffractometer containing Cu K_α at 45 KV 40 mA as the source of X-rays was used for the determination of crystal structure and purity of nanoalloys. Topographical features, compositional mapping, phase distribution and morphology of samples were accessed by scanning electron microscopy (SEM)- JEOL JSM-840. Sensing application of these grown nanoalloys was studied by electrochemical techniques viz. cyclic voltammetry (CV) and electrochemical impedance spectroscopy (EIS) by using Autolab PGSTAT 302 potentiostat/galvanostat electrochemical workstation. Electrochemical cell used for CV and EIS experiments was comprised of a double-walled glass container (30 mL) equipped with Ag NPs and Ad-Cu nanoalloys modified glassy carbon electrode (GCE) as working electrode, Pt wire as counter electrode, and Ag/AgCl as reference electrode. EIS experiments have been performed by applying frequency from 10 mHz to 100 kHz and total 30 different frequencies were used to record the impedance response. Frequency response analyzer (FRA) software has been used for EIS experiments and data analysis. This software uses Levenberg-Marquardt algorithm. The fitting procedure changes the values of the parameters until the mathematical function matches the experimental data within a certain error margin. The goodness of the fit

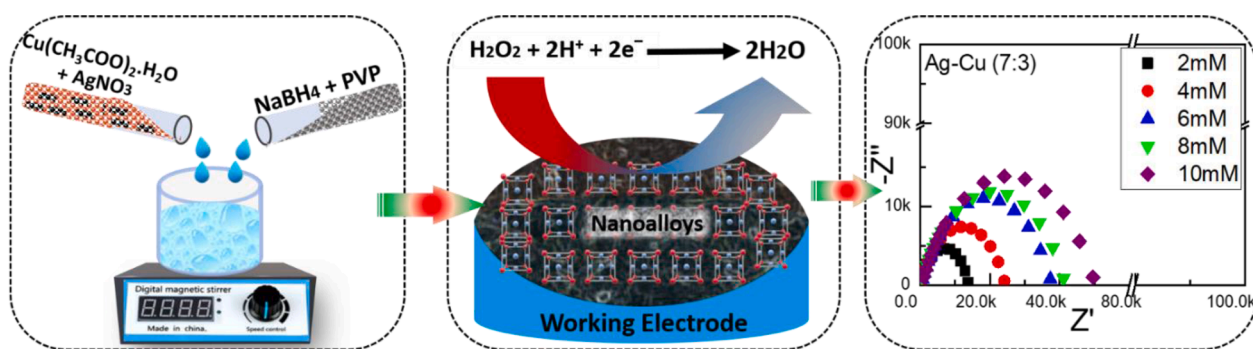


Fig. 1. Fabrication and working of Ag-Cu nanoalloys-based electrochemical sensor.

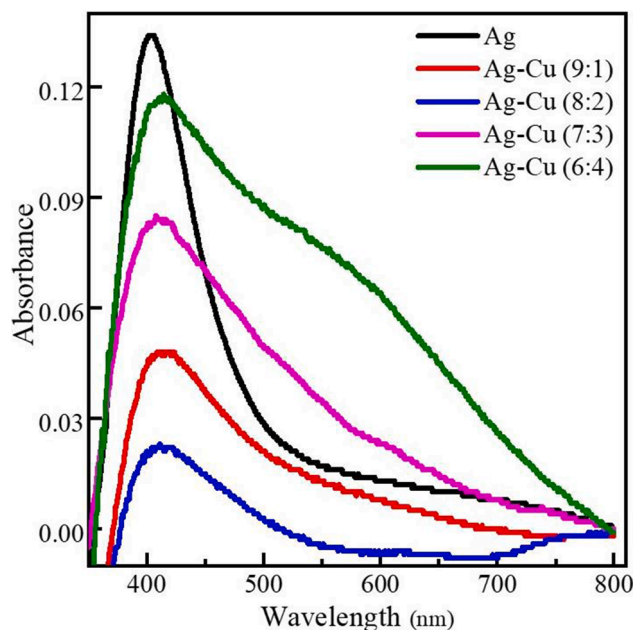


Fig. 2. UV/Visible spectra of 3.3 mM aqueous solutions of Ag nanoparticles, Ag-Cu (9:1), Ag-Cu (8:2), Ag-Cu (7:3), and Ag-Cu (6:4) nanoalloys.

was characterized by the value of χ^2 (chi-squared). For all measurements, values of circuit elements were measured with $\chi^2 < 0.01$.

2.3. Fabrication of working electrode

The glassy carbon was modified with Ag nanoparticles and Ag-Cu nanoalloys by a previously reported method [46]. Briefly, before the deposition of material on the GCE surface, the electrode was thoroughly cleaned by polishing with alumina slurry (0.05 μm) on the rubber pad for few minutes and then washed several times with DI water

thoroughly. After this, the electrode was ultrasonically cleaned successively with ethanol and DI for 10 min in each case. The electrode was then dried and used for the deposition of material immediately. Then 2 mg of material i.e. Ag NPs or Ag-Cu nanoalloys was poured into 1 mL of DI water and the mixture was sonicated for 10 min until the particles become suspended in the water. The particles were then deposited on GCE surface by casting 5 μL suspensions on GCE surface. The electrode was then dried in oven at 40 $^\circ\text{C}$ under argon environment. This process was repeated three to four times until a uniform layer of particles is formed on the surface of GCE. To deposit the as grown material on the surface of GCE, a 5 μL solution of Nafion was casted and then dried in the oven at 40 $^\circ\text{C}$ overnight under argon environment.

3. Results and discussions

3.1. Structural studies

Fabrication and working of Ag-Cu nanoalloys-based electrochemical sensor towards H_2O_2 detection is shown in Fig. 1.

Formation of as synthesised nanoparticles has been assessed by UV-Visible absorption spectra of pure Ag nanoparticles and Ag-Cu nanoalloys as shown in Fig. 2. Pure Ag nanoparticles show a strong absorption peak at 403 nm, whereas Ag-Cu nanoalloys Ag-Cu (9:1), Ag-Cu (8:2), Ag-Cu (7:3), and Ag-Cu (6:4) exhibit their absorption peaks at wavelengths of 411, 412, 413, and 414 nm, respectively. These peaks are attributed to localized surface plasmon resonance, which can be assessed by Mie resonance condition [47]. Surface plasmon bands of Ag-Cu nanoalloys are at the middle of the maximum absorption spectra of Ag (at 403 nm) and Cu (at 545 nm) nanoparticles [48]. For Ag-Cu nanoalloys, there is a regular peak shift of 1 nm towards the longer wavelength (red shift) with increasing copper contents. This red shift in maximum absorption values of Ag-Cu nanoalloys is due to the increase in refractive index of the medium and is according to the literature values [47]. It has further been observed that the optical density decreases with increasing concentration of Cu (up to Ag-Cu (8:2)) and it is due to agglomeration of the nanoparticles and compactness in packing

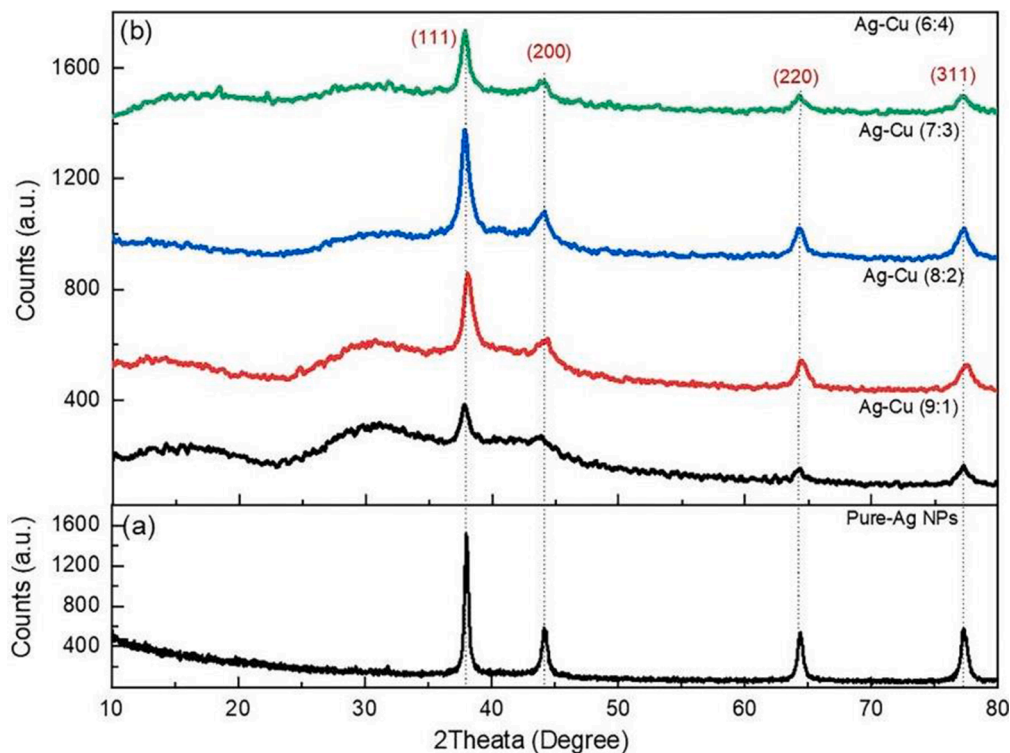


Fig. 3. X-ray diffraction spectra of (a) pure Ag NPs and (b) Ag-Cu (9:1), Ag-Cu (8:2), Ag-Cu (7:3), and Ag-Cu (6:4) nanoalloys.

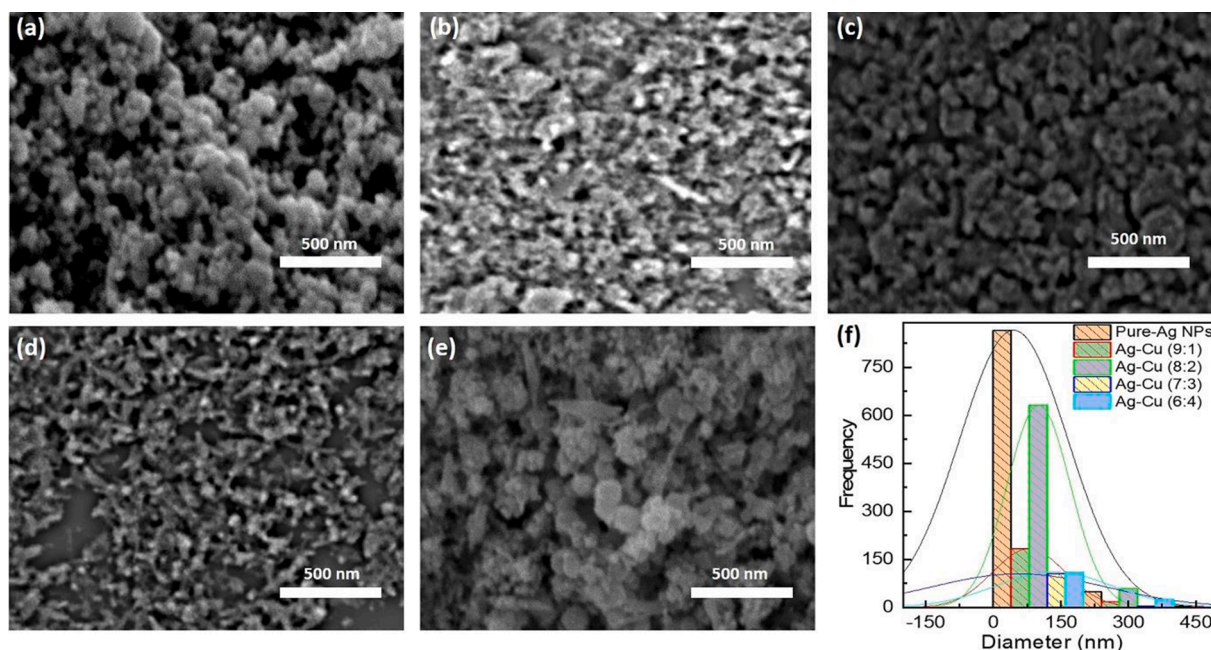


Fig. 4. SEM micrographs of (a) pure Ag NPs, (b) Ag-Cu (9:1), (c) Ag-Cu (8:2), (d) Ag-Cu (7:3), and Ag-Cu (6:4) nanoalloys, (f) particles size distribution computed by using image-J.

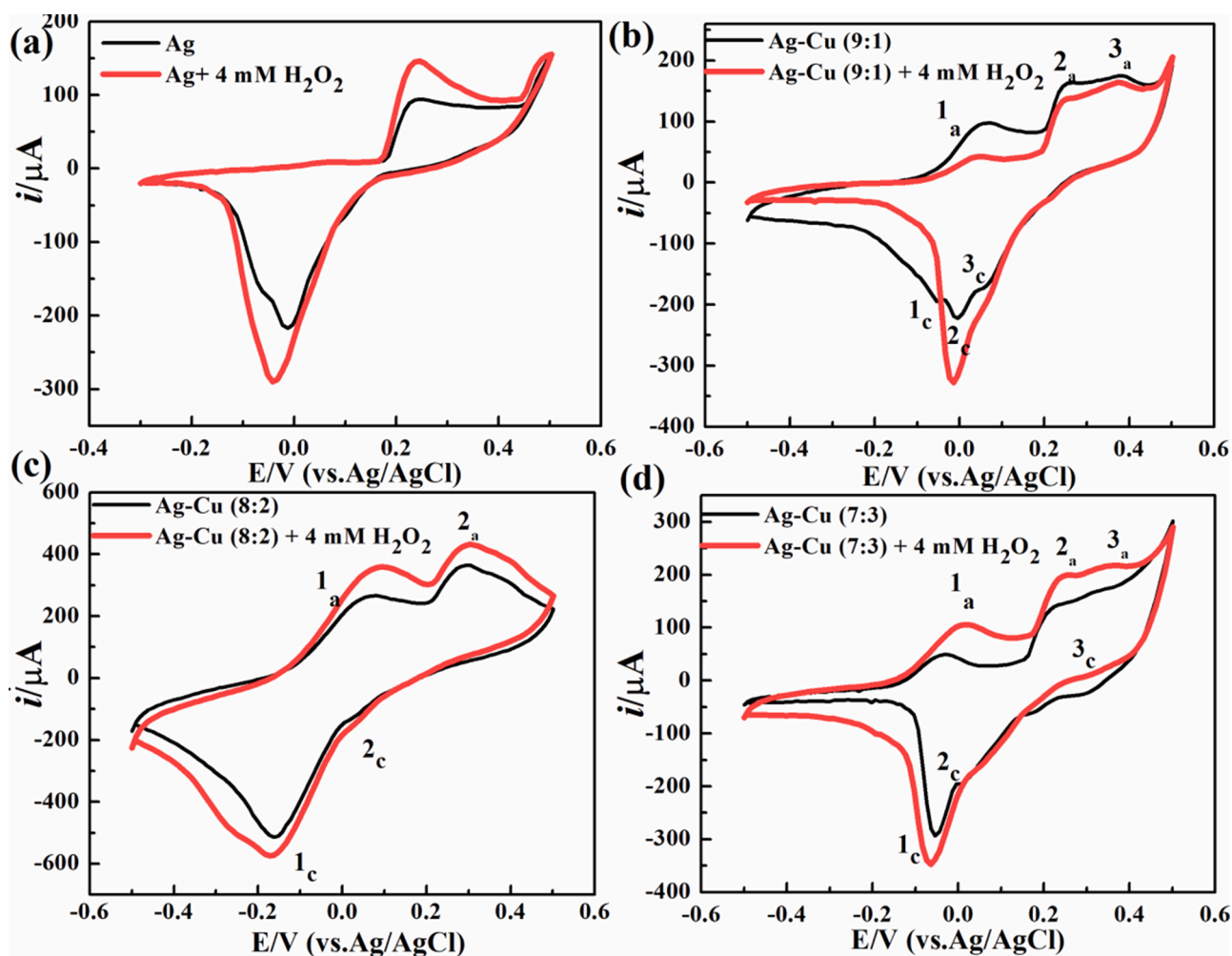


Fig. 5. Cyclic voltammograms of (a) pure Ag NPs (b) Ag-Cu (9:1), (c) Ag-Cu (8:2), and (d) Ag-Cu (7:3) nanoalloys modified GCE at scan rate of 50 mV/s in phosphate buffer solution of pH 7.4 in the absence and presence of 4 mM H_2O_2 at room temperature.

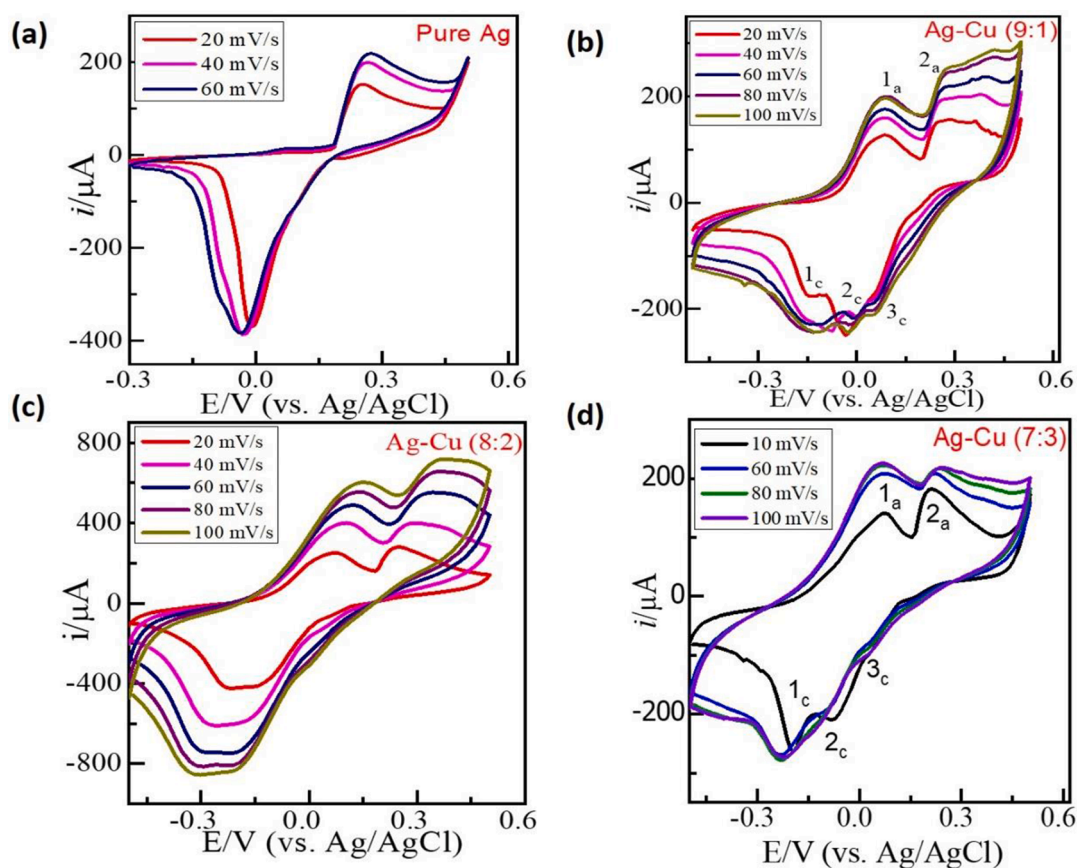


Fig. 6. Cyclic voltammograms of (a) pure Ag NPs (b) Ag-Cu (9:1), (c) Ag-Cu (8:2), and (d) Ag-Cu (7:3) nanoalloy modified GCE at various scan rates in phosphate buffer solution of pH 7.4 at room temperature.

[49,50]. This shows that the optical density not only depends upon size of the NPs but also the compactness in packing. However, further increase of Cu contents results in enhanced absorbance values which is due to increase in homogeneity of nanoalloys [50]. It can further be seen from the spectra that as the copper contents increases in Ag-Cu nanoalloys, absorption peaks become broadened [51]. Overall, these observations indicate the formation of Ag-Cu nanoalloys instead of separate Ag and Cu nanoparticles, otherwise double peak spectrum would have been resulted [52].

In order to confirm the crystal structure of the pure Ag NPs and Ag-Cu nanoalloys, XRD measurements were performed as shown in Fig. 3. These XRD spectra reveal that diffraction peaks of Ag-Cu nanoalloys are located at $2\theta = 38^\circ, 44.5^\circ, 64.5^\circ$ and 77.5° corresponding to the planes (111), (002), (022), and (113) which are similar to that of pure Ag NPs. It eventually confirms the fabrication of nanoalloys in which copper atoms have positioned themselves among face centered cubic crystal structure of silver atoms rather than individual silver and copper NPs. However, with increasing Cu contents there is a slight shift in peak position of (111) peak towards higher 2θ value and a maximum shift of 0.5° has been observed for Ag-Cu (8:4) nanoalloy. This observation indicates the complete dissolution of Cu atoms within the face centered cubic lattice and does not result in any additional peaks of Cu [53,54]. Hikmah et al. reported synthesis of silver-copper core-shell nanoparticles and observed very low intensity diffraction peaks of (111), (200) and (220) planes for Ag-Cu (8:2) and (8:3 M) compositions and no Cu peak for 8:4 M composition [55]. However, in present case to explain the absence of any diffraction peaks for Cu, another possible reason is diffraction peaks for Cu metal are too small to be observed. Due to the incorporation of copper atoms within the crystal structure of silver, a slight broadening of peaks has been observed [56]. The magnitude of lattice constant and mean crystallite size of pure silver nanoparticles is

found to be 4.045 \AA and 29 nm, respectively. From Scherer's equation, the average crystallite sizes for Ag-Cu nanoalloys have been found in the range of 13 to 22 nm which reveals that on alloying, the crystallite size decreases but (111) orientation is most favourable for the nanoalloys. It is also noted that the XRD peaks are somewhat broadened as the crystallite size decreases. The values of interplanar spacing (d_{hkl}) for Ag NPs calculated from the XRD spectra are 2.366, 2.048, 1.44 and 1.233 \AA which are in excellent agreement with standard values (JCPDS PDF card 04-0783).

Scanning electron microscopy (SEM) was used to study the structural morphology of the prepared nanomaterials. SEM images of pure Ag nanoparticles and Ag-Cu alloy nanoparticles in different ratios i.e. 9:1, 8:2, 7:3, 6:4 are shown in Fig. 4 (a-e). Fig. 4(f) shows the particles size distribution of the NPs, and shows that the pure Ag NPs have uniform spherical symmetries while addition of Cu contents increases the size of the particles and results in agglomeration of particles. It has been observed from the SEM micrographs that average sizes of particles for all the compositions are in the range of 50 to 80 nm. However, some larger sized particles in the range of 200 to 250 nm have also been found. Mostly the particles are spherical in morphology and look agglomerated in almost all the compositions. This condensation of particles has also been confirmed from UV-Visible results (Fig. 2).

3.2. Electrochemical performance evaluation

The electrochemical performance of all samples has been investigated by cyclic voltammetry (CV) and electrochemical impedance spectroscopy (EIS). The fabricated samples (pure Ag and nanoalloys of Ag-Cu with various ratios) modified glassy carbon electrode (GCE) was used in all CV and EIS experiments. All CV experiments have been recorded in phosphate buffer solution of pH 7.4 in the absence and

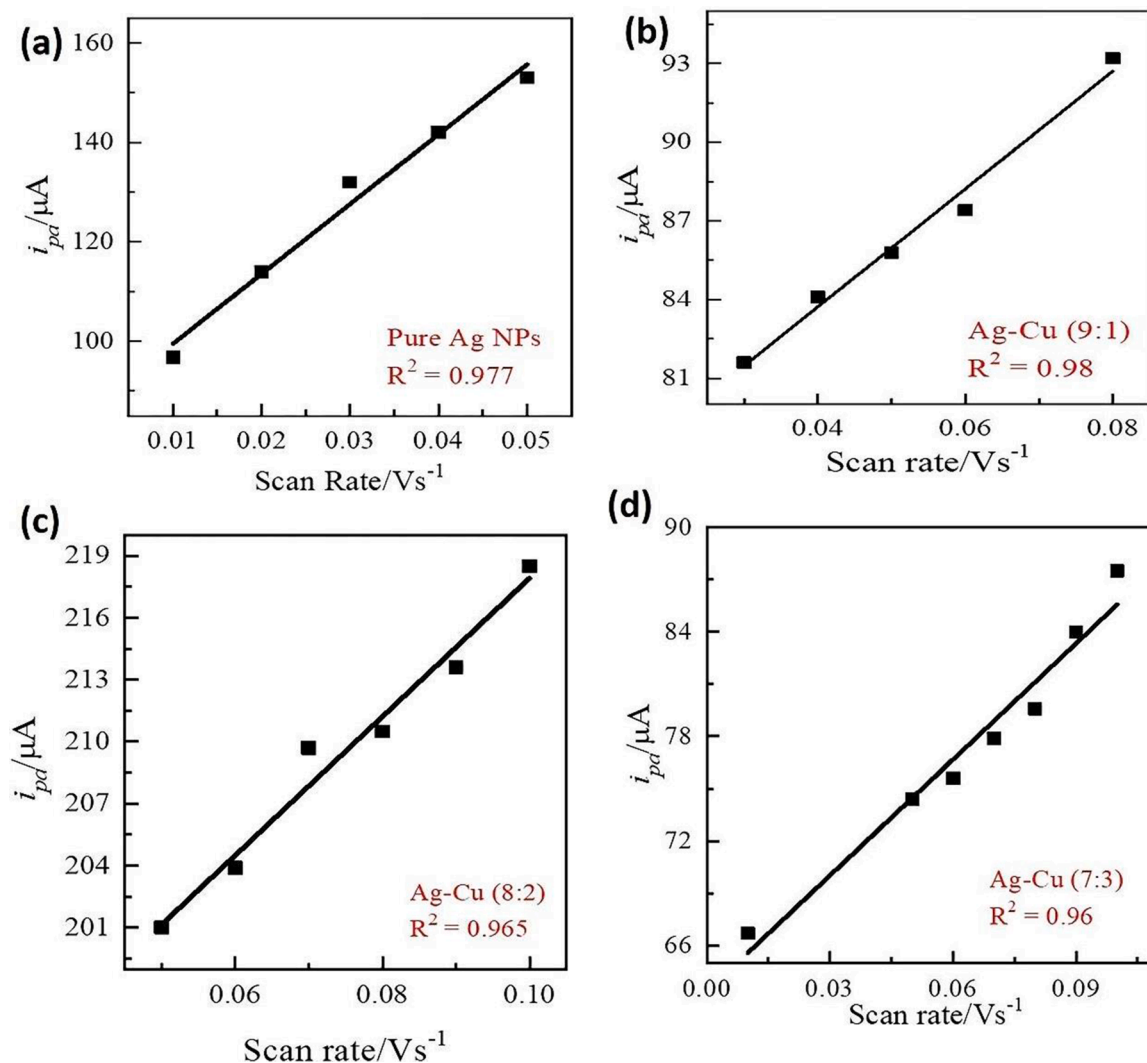


Fig. 7. Variation of i_{pa} with scan rate for (a) pure Ag NPs (b) Ag-Cu (9:1), (c) Ag-Cu (8:2), and (d) Ag-Cu (7:3) modified GCE.

presence of H_2O_2 . CV has been used to analyze the adsorption behavior of prepared sensors on GCE and to get initial guess about their sensing potential for H_2O_2 . CVs recorded on Ag NPs and Ag-Cu nanoalloys (9:1, 8:2 and 7:3) modified GCE in phosphate buffer solution of pH 7.4 in the absence and presence of H_2O_2 are presented in Fig. 5(a-d). For pure Ag NPs, anodic and cathodic peak potentials are 0.23 and -0.01 V and their corresponding anodic and cathodic peak currents are 93 and -213 μA , respectively. For Ag-Cu (9:1) nanoalloys, three anodic peaks designated as 1_a , 2_a , and 3_a at 0.05, 0.25, and 0.37 V with corresponding anodic peak currents 197, 145, and 97 μA , respectively, have been observed. Three cathodic peaks designated as 1_c , 2_c , and 3_c at -0.05 , -0.005 , and 0.06 V, with corresponding cathodic peak currents -5 , -270 , and -7 μA , respectively, have also been observed. For Ag-Cu (8:2) nanoalloys, two anodic peaks designated as 1_a and 2_a at 0.05 and 0.29 V with corresponding anodic peak currents 80 and 145 μA , respectively, have been observed. Two cathodic peaks designated as 1_c and 2_c at -0.16 and 0.02 V, with corresponding cathodic peak currents -265 and -0.02 μA , respectively, have also been observed. For Ag-Cu (7:3) nanoalloys, three anodic peaks designated as 1_a , 2_a , and 3_a at -0.03 , 0.23, and 0.35 V with corresponding anodic peak currents 90, 40, and 0.04 μA , respectively, have been observed. Three cathodic peaks designated as 1_c , 2_c , and 3_c at -0.05 , 0.02, and 0.28 V, with corresponding cathodic peak currents -260 , -45 , and -3 μA , respectively, have also been observed. It is clear from the CV curves in Fig. 5 (a-d) that addition of H_2O_2 results in improvement of peak currents for all the sensors. For Ag NPs, it has been

noticed that in the presence of H_2O_2 in Fig. 5(a), peak currents of both anodic and cathodic peaks are significantly enhanced. This increase in peak currents is attributed to catalytic reactions taking place on Ag NPs surface. Additionally, it has been found that anodic peak potential is shifted towards more positive potential while cathodic peak potential is shifted towards more negative potential due to H_2O_2 . It can be inferred from these observations that Ag NPs may be used as sensor for H_2O_2 determination.

Form cyclic voltammograms of Ag-Cu (9:1) nanoalloy (Fig. 5b), it can be observed that with the addition of H_2O_2 , peak currents of oxidation peaks for copper (1_a) and silver (2_a) are decreased whereas the peak current of reduction peak for silver (2_c) is significantly enhanced. It is very clear from these observations that in the presence of H_2O_2 , reduction peak current in CV signal of Ag-Cu (9:1) nanoalloys is significantly enhanced. Similarly, for Ag-Cu (8:2), Ag-Cu (7:3) nanoalloys (Fig. 5c and d), presence of H_2O_2 results in enhanced reduction peak currents in their CVs. It is pertinent to mention that for all the sensors in the presence of H_2O_2 , reduction peaks are merged into a single peak at -0.04 , -0.01 , -0.16 , and -0.07 V for Ag, Ag-Cu (9:1), Ag-Cu (8:2), Ag-Cu (7:3), respectively, with enhanced cathodic peak current. The values of reduction peak currents are -350 , -370 , -295 and -281 μA for Ag, Ag-Cu (9:1), Ag-Cu (8:2), Ag-Cu (7:3), respectively. The increase in reduction peak current for all the nanoalloys is attributed to the catalytic reduction of H_2O_2 [57]. It has further been noticed that cathodic peak potentials for Ag-Cu alloys are slightly shifted towards

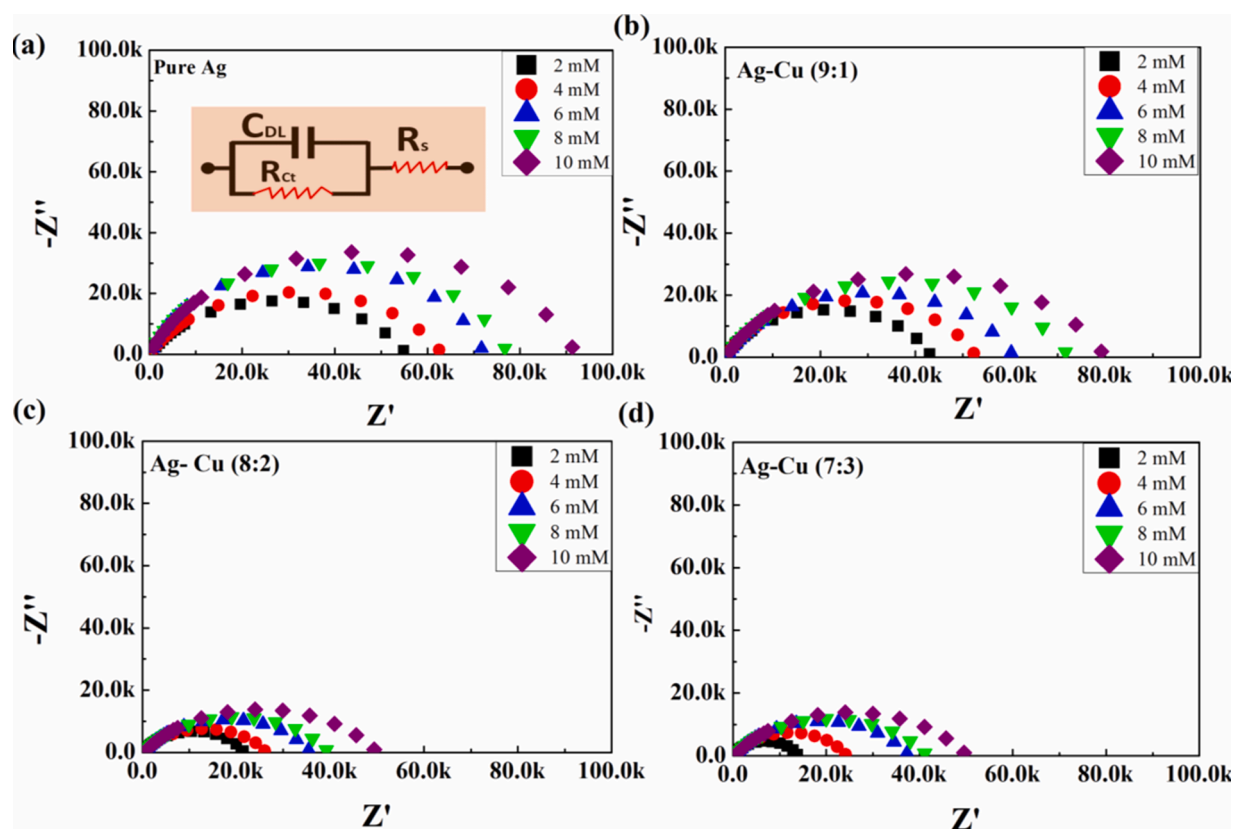


Fig. 8. Electrochemical impedance spectra (Nyquist plots) of (a) pure Ag NPs (b) Ag-Cu (9:1), (c) Ag-Cu (8:2), and (d) Ag-Cu (7:3) modified GCE at various concentrations of H_2O_2 .

more negative potential in the presence of H_2O_2 . Similarly, anodic peak potentials are also slightly shifted towards more positive potential in the presence of H_2O_2 . Thus, it can be concluded on the basis of above observations that Ag-Cu (9:1), Ag-Cu (8:2), Ag-Cu (7:3) may be used as a sensing material for the determination of H_2O_2 in solution.

To get insight into adsorption of Ag NPs and Ag-Cu nanoalloys on GCE, CV experiments have been performed at different scan rates in phosphate buffer solution of pH 7.4 and resultant CVs of Ag, Ag-Cu (9:1), Ag-Cu (8:2) and Ag-Cu (9:3) are shown in Fig. 6. A straight-line plot of peak current vs. scan rate instead of peak current vs. square root of scan rate have been observed for all the sensors (Fig. 7). This behavior clearly indicates strong adsorption of sensor materials on GCE and shows successful modification of GCE with said materials [58]. It can also be observed from the CVs that the increase in scan rate, peaks become broadened and merged. This is due to the strong adsorption of samples on GCE.

Additionally, electrochemical impedance spectroscopy (EIS) curves were employed to obtain impedance values at the interface between catalysts and electrolytes. EIS results demonstrate that for each catalyst, modified GCE has larger charge transfer resistance value ($> 13 \text{ K } \Omega$) than that for the bare (pure) GCE which ($13 \text{ K } \Omega$) which suggests the successful modification of GCE with nanoalloys. The results obtained by EIS are consistent with the results tested by CV.

In order to study the effect of H_2O_2 concentration on the impedance response, EIS was performed in phosphate buffer solution of pH 7.4 in the presence of varying concentrations of H_2O_2 from 2.0 to 10.0 mM. The applied frequency was from 10 mHz to 100 kHz. The Nyquist plots of the impedance response form Ag NPs modified GCE in phosphate buffer solution of pH 7.4 in the absence and presence of different H_2O_2 concentrations is shown in Fig. 8(a).

The Nyquist plots of Ag-Cu (9:1), Ag-Cu (8:2), and Ag-Cu (7:3) nanoalloys modified GCE in pure phosphate buffer solution and with

different H_2O_2 concentrations are shown in Fig. 8(b-d). The R_{ct} values were similarly calculated by fitting the impedance data into same equivalent circuit used for pure Ag NPs. In order to determine the charge transfer resistance (R_{ct}) value, the impedance data (obtained semi-circles) was fitted into an equivalent circuit. It has been observed that the R_{ct} value increases with increasing H_2O_2 concentration. The linear dependence of R_{ct} values on concentration of H_2O_2 is depicted in Fig. 9 (a) and this curve has been used for the quantification of H_2O_2 .

Again, it has been found that the R_{ct} values increase with increasing H_2O_2 concentration, which shows that R_{ct} is a concentration dependent parameter and can be used for the quantitative detection of H_2O_2 . The linear dependence of R_{ct} values with increasing concentrations of H_2O_2 for Ag-Cu (9:1), Ag-Cu (8:2), and Ag-Cu (7:3) nanoalloys are depicted in Fig. 9 (b-d). Among all the compositions, Ag-Cu (9:1) nanoalloy has shown the best sensing performance towards detection of H_2O_2 having LOD of $152 \mu\text{M}$, LOQ of $508 \mu\text{M}$, and linear regression co-efficient R^2 of 0.996. Fig. 10 shows the graphical representation of LOD and LOQ for the various nanoalloys. We notice that the LOD varies from 152 to 190 μM , whereas the nanoalloy with composition of 9:1 shows the best LOD approaching to 152 μM while the highest is 190 μM for 8:2 compositions, when exposed to H_2O_2 solution. On the other hand, limit of quantification varies from 508 to 633 μM , again the sample with best detection limit exhibits quantification limit of 508 μM , while 8:2 composition exhibits highest value of limit of quantification which is 633 μM .

Compared with other nanocomposites as mentioned in the Table 1, nanoalloys base on Ag-Cu show significantly enhanced detection of H_2O_2 . Our sensor based on Ag-Cu (9:1) nanoalloy demonstrates the best LOD. The linear range of our fabricated nanoalloys is wide enough which is acceptable in several situations. This can be explained by the fact that due to the highly ordered structure and uniform distribution; each nanoparticle can catalyze the reduction of H_2O_2 and contribute to the

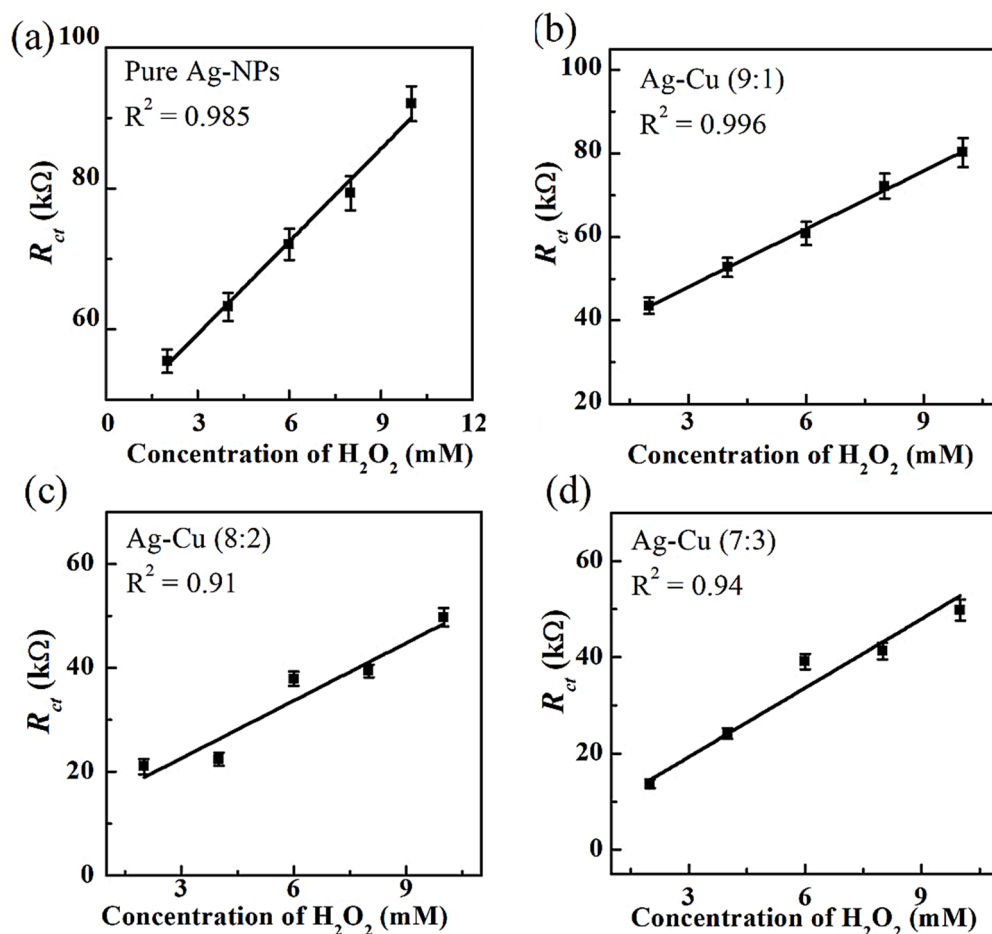


Fig. 9. The sensing performance for (a) pure Ag NPs (b) Ag-Cu (9:1), (c) Ag-Cu (8:2), and (d) Ag-Cu (7:3) nanoalloys modified GCE at various concentrations of H_2O_2 .

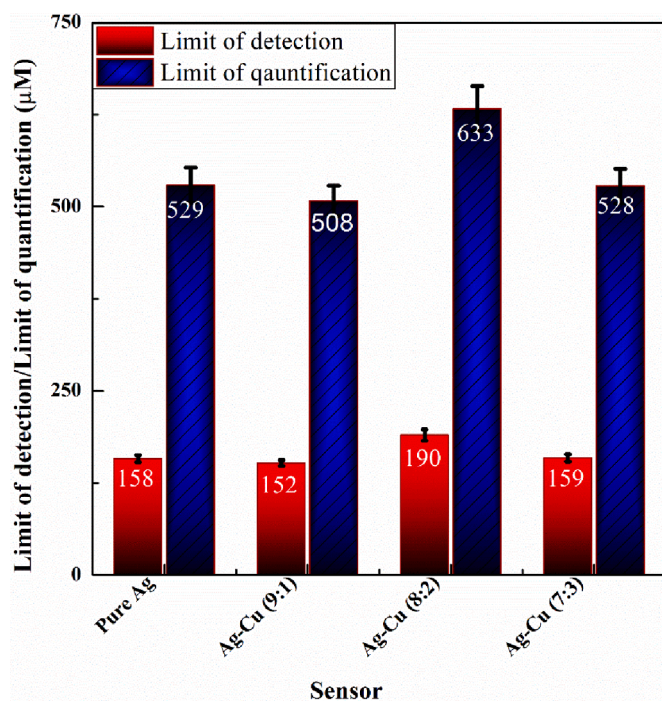


Fig. 10. Comparison of the limit of detection/quantification for pure Ag NPs, Ag-Cu (9:1), Ag-Cu (8:2), and Ag-Cu (7:3) nanoalloys.

Table 1

Comparison of H_2O_2 detection by different electrochemical sensors.

Electrodes	Linear Range (μM)	LOD (μM)	Correlation Coefficient (R^2)	Refs.
Metal doped CNT	300–750	430	0.998	[59]
SWCNTs	1900–2400	1000	0.99	[60]
Ag-Au/ Cu_2O	3180–20,780	1300	0.994	[61]
Ag-Cu nanoalloys		152	0.996	This work

electrochemical performance. Also, because these nanoalloys are attached to the substrate directly, electrochemical signals can be effectively transferred and collected by the analysis system. By increasing the length and surface roughness, the enlarged electroactive surface area can enhance the sensing ability, leading to higher sensitivity and lower LOD.

4. Conclusions

In summary, Ag NPs and Cu nanoalloys were synthesized by using facile chemical reduction method under inert environment using PVP as capping and stabilizing agent. The sensing activity of Ag NPs and Ag-Cu nanoalloys modified GCEs towards H_2O_2 was checked by using CV and EIS which revealed that modified GCEs exhibit good sensing activity towards H_2O_2 in a range of concentrations from 2.0 to 9.61 mM H_2O_2 . Because of the large surface and strong electron coupling, excellent electrochemical sensing activity has been achieved. The comparison of

the sensing performance of the pure Ag NPs and different Ag-Cu nanoalloys towards H₂O₂ has been studied. Interestingly, nanoalloy with composition of Ag-Cu (9:1) demonstrates highest LOD of 152 μM, with R² value of 0.996. Such sensor is suitable for the detection of H₂O₂ released from living cell.

CRedit authorship contribution statement

Muhammad Shafa: Conceptualization, Writing – original draft. **Iqbal Ahmad:** Supervision, Validation. **Shahid Hussain:** Funding acquisition, Validation, Resources. **Muhammad Asif:** Visualization, Validation. **Yi Pan:** Methodology. **Rustem Zairov:** Data curation, Software. **Asma A. Alothman:** Validation. **Mohamed Ouladsmame:** Resources. **Zahid Ullah:** Formal analysis, Investigation. **Nabi Ullah:** Formal analysis. **Chen Lai:** Visualization, Validation. **Uzma Jabeen:** Formal analysis, Investigation.

Declaration of Competing Interest

The authors declare that they have no known competing financial interests or personal relationships that could have appeared to influence the work reported in this paper.

Data availability

No data was used for the research described in the article.

Acknowledgments

M. Shafa and Y. Pan acknowledge the support from the China Postdoctoral Science Foundation Grant No. 2019M663691. This work was funded by the Researchers Supporting Project Number (RSP-2021/243) King Saud University, Riyadh, Saudi Arabia. This work was also supported by National Natural Science Foundation of China Grant No. 51950410596. This work has also been supported by the Kazan Federal University Strategic Academic Leadership Program (PRIORITY-2030).

References

- Y. Li, K. Huan, D. Deng, L. Tang, J. Wang, L. Luo, Facile synthesis of ZnMn₂O₄@rGO microspheres for ultrasensitive electrochemical detection of hydrogen peroxide from human breast cancer cells, *ACS Appl. Mater. Interfaces* 12 (3) (2020) 3430–3437.
- A. Vigliocco, Z. Del Bel, M.V. Perez-Chaca, A. Molina, F. Zirulnik, A.M. Andrade, S. Alemano, Spatiotemporal variations in salicylic acid and hydrogen peroxide in sunflower seeds during transition from dormancy to germination, *Physiol. Plant.* 169 (1) (2020) 27–39.
- G.J. Ahammed, X. Li, Y. Yang, C. Liu, G. Zhou, H. Wan, Y. Cheng, Tomato WRKY81 acts as a negative regulator for drought tolerance by modulating guard cell H₂O₂-mediated stomatal closure, *Environ. Exp. Bot.* 171 (2020), 103960.
- A. Amer, T. Shoala, Physiological and phenotypic characters of sweet marjoram in response to pre-harvest application of hydrogen peroxide or chitosan nanoparticles, *Sci. Hortic.* 268 (2020), 109374.
- J. Shah, A. Pandya, P. Goyal, S.K. Misra, S. Singh, BSA-decorated magnesium nanoparticles for scavenging hydrogen peroxide from human hepatic cells, *ACS Appl. Nano Mater.* 3 (4) (2020) 3355–3370.
- M. Lu, X. Zhang, J. Zhao, Q. You, Z. Jiang, A hydrogen peroxide responsive prodrug of Keap1-Nrf2 inhibitor for improving oral absorption and selective activation in inflammatory conditions, *Redox. Biol.* 34 (2020), 101565.
- A.R. Gibson, B.R. O'Leary, J. Du, E.H. Sarsour, A.L. Kalen, B.A. Wagner, J. M. Stolwijk, K.C. Falls-Hubert, M.S. Alexander, R.S. Carroll, D.R. Spitz, G. R. Buettner, P.C. Goswami, J.J. Cullen, Dual oxidase-induced sustained generation of hydrogen peroxide contributes to pharmacologic ascorbate-induced cytotoxicity, *Cancer Res.* 80 (7) (2020) 1401–1413.
- S. Chinnapaka, G. Zheng, A. Chen, G. Munirathinam, Nitro aspirin (NCX4040) induces apoptosis in PC3 metastatic prostate cancer cells via hydrogen peroxide (H₂O₂)-mediated oxidative stress, *Free Radic. Biol. Med.* 143 (2019) 494–509.
- L. Qi, Q. Hu, Q. Kang, L. Yu, Fabrication of liquid-crystal-based optical sensing platform for detection of hydrogen peroxide and blood glucose, *Anal. Chem.* 90 (19) (2018) 11607–11613.
- S.A. Kitte, M.N. Zafar, Y.T. Zholudov, X. Ma, A. Nsabimana, W. Zhang, G. Xu, Determination of concentrated hydrogen peroxide free from oxygen interference at stainless steel electrode, *Anal. Chem.* 90 (14) (2018) 8680–8685.
- K.M. Tripathi, H.T. Ahn, M. Chung, X.A. Le, D. Saini, A. Bhati, S.K. Sonkar, M. I. Kim, T. Kim, N. S, and P-Co-doped carbon quantum dots: intrinsic peroxidase activity in a wide pH range and its antibacterial applications, *ACS Biomater. Sci. Eng.* 6 (10) (2020) 5527–5537.
- Q. Wang, X. Zhang, X. Chai, T. Wang, T. Cao, Y. Li, L. Zhang, F. Fan, Y. Fu, W. Qi, An electrochemical sensor for H₂O₂ based on Au nanoparticles embedded in UiO-66 metal-organic framework films, *ACS Appl. Nano Mater.* 4 (6) (2021) 6103–6110.
- B. Gokcal, C. Kip, D. Sahinbas, E. Celik, A. Tuncel, Silica microspheres functionalized with the iminodiacetic acid/copper(II) complex as a peroxidase mimic for use in metal affinity chromatography-based colorimetric determination of histidine-tagged proteins, *Mikrochim. Acta* 187 (2) (2020) 121.
- J. Lu, H. Zhang, S. Li, S. Guo, L. Shen, T. Zhou, H. Zhong, L. Wu, Q. Meng, Y. Zhang, Oxygen-vacancy-enhanced peroxidase-like activity of reduced Co₃O₄ nanocomposites for the colorimetric detection of H₂O₂ and glucose, *Inorg. Chem.* 59 (5) (2020) 3152–3159.
- H. Saada, R. Abdallah, J.F. Bergamini, S. Fryars, V. Dorcet, L. Joanny, F. Gouttefangeas, S. Ollivier, G. Loget, Photoelectrochemical sensing of hydrogen peroxide on hematite, *ChemElectroChem* 7 (5) (2020) 1155–1159.
- H. Wu, R. Nissler, V. Morris, N. Herrmann, P. Hu, S.J. Jeon, S. Kruss, J.P. Giraldo, Monitoring plant health with near-infrared fluorescent H₂O₂ nanosensors, *Nano Lett.* 20 (4) (2020) 2432–2442.
- C. Chen, D. Xiong, M. Gu, C. Lu, F.Y. Yi, X. Ma, MOF-derived bimetallic CoFe-PBA composites as highly selective and sensitive electrochemical sensors for hydrogen peroxide and nonenzymatic glucose in human serum, *ACS Appl. Mater. Interfaces* (2020).
- S.H. Wu, X.B. Huang, Y. Tang, L.M. Ma, Y. Liu, J.J. Sun, Temperature controllable electrochemical sensors based on horseradish peroxidase as electrocatalyst at heated Au disk electrode and its preliminary application for H₂O₂ detection, *Anal. Chim. Acta* 1096 (2020) 44–52.
- S. Ramaraj, M. Sakthivel, S.M. Chen, B.S. Lou, K.C. Ho, Defect and additional active sites on the basal plane of manganese-doped molybdenum diselenide for effective enzyme immobilization: *in vitro* and *in vivo* real-time analyses of hydrogen peroxide sensing, *ACS Appl. Mater. Interfaces* 11 (8) (2019) 7862–7871.
- J. Meier, E.M. Hofferber, J.A. Stapleton, N.M. Iverson, Hydrogen peroxide sensors for biomedical applications, *Chemosensors* 7 (4) (2019) 64.
- J.N.O. Amu-Darko, S. Hussain, Q. Gong, X. Zhang, Z. Xu, M. Wang, G. Liu, G. Qiao, Highly sensitive In₂O₃/PANI nanosheets clusters-based gas sensor for NO₂ detection, *J. Environ. Chem. Eng.* 11 (2023) 109211, <https://doi.org/10.1016/j.jece.2022.109211>.
- H. Wang, Y. Li, M. Yang, P. Wang, Y. Gu, FRET-Based upconversion nanoprobe sensitized by Nd(3+) for the ratiometric detection of hydrogen peroxide *in vivo*, *ACS Appl. Mater. Interfaces* 11 (7) (2019) 7441–7449.
- Y. Zhao, A new era of metal-organic framework nanomaterials and applications, *ACS Appl. Nano Mater.* 3 (6) (2020) 4917–4919.
- M.A. Boles, M. Engel, D.V. Talapin, Self-assembly of colloidal nanocrystals: from intricate structures to functional materials, *Chem. Rev.* 116 (18) (2016) 11220–11289.
- S. Manzoor, T. Munawar, S. Goudria, M. Sadaqat, A.G. Abid, A. Munawar, F. Hussain, F. Iqbal, I. Ahmad, M.N. Ashiq, Nanopetals shaped CuNi alloy with defects abundant active surface for efficient electrocatalytic oxygen evolution reaction and high performance supercapacitor applications, *J. Energy Storage* 55 (2022), 105488.
- R.S. Gohar, I. Ahmad, A. Shah, S. Majeed, M. Najam-Ul-Haq, M.N. Ashiq, Fabrication of transition-metal oxide and chalcogenide nanocrystals with enhanced electrochemical performances, *J. Energy Storage* 31 (2020), 101621.
- S. Biswas, Y. Chen, Y. Xie, X. Sun, Y. Wang, Ultrasmall Au(0) inserted hollow PCN-222 MOF for the high-sensitive detection of estradiol, *Anal. Chem.* 92 (6) (2020) 4566–4572.
- N.A. Khan, N. Rashid, I. Ahmad, Zahidullah, R. Zairov, H.u. Rehman, M.F. Nazar, U. Jabeen, An efficient Fe₂O₃/FeS heterostructures water oxidation catalyst, *Int. J. Hydrog. Energy* 47 (53) (2022) 22340–22347.
- N.A. Khan, I. Ahmad, N. Rashid, M.N. Zafar, F.K. Shehzad, Z. ullah, A. Ul-Hamid, M.F. Nazar, M. Junaid, M. Faheem, S.S. Shafqat, U. Jabeen, A. Dahshan, Enhanced electrochemical activity of Co₃O₄/Co₉S₈ heterostructure catalyst for water splitting, *Int. J. Hydrog. Energy* 47 (72) (2022) 30970–30980.
- I. Ahmad, J. Ahmed, S. Batool, M.N. Zafar, A. Hanif, Zahidullah, M.F. Nazar, A. Ul-Hamid, U. Jabeen, A. Dahshan, M. Idrees, S.A. Shehzadi, Design and fabrication of Fe₂O₃/FeP heterostructure for oxygen evolution reaction electrocatalysis, *J. Alloy. Compd.* 894 (2022), 162409.
- J. Xuan, X.-d. Jia, L.-P. Jiang, E.S. Abdel-Halim, J.-J. Zhu, Gold nanoparticle-assembled capsules and their application as hydrogen peroxide biosensor based on hemoglobin, *Bioelectrochemistry* 84 (2012) 32–37.
- S. Zhang, R. Geryak, J. Geldmeier, S. Kim, Synthesis, assembly, and applications of hybrid nanostructures for biosensing, *Chem. Rev.* 117 (20) (2017) 12942–13038.
- A.A. Menazea, M.K. Ahmed, Silver and copper oxide nanoparticles-decorated graphene oxide via pulsed laser ablation technique: preparation, characterization, and photoactivated antibacterial activity, *Nano-Struct. Nano-Objects* 22 (2020), 100464.
- A.A. Menazea, Synthesis and antibacterial activity of graphene oxide decorated by silver and copper oxide nanoparticles, *J. Mol. Struct.* 1218 (2020), 128536.
- S. Varagnolo, J. Lee, H. Amari, R.A. Hattton, Selective deposition of silver and copper films by condensation coefficient modulation, *Mater. Horiz.* 7 (1) (2020) 143–148.
- A. Ali, V. Baheti, M. Vik, J. Militky, Copper electroless plating of cotton fabrics after surface activation with deposition of silver and copper nanoparticles, *J. Phys. Chem. Solids* 137 (2020), 109181.

- [37] C. Huang, X. Chen, Z. Xue, T. Wang, Effect of structure: a new insight into nanoparticle assemblies from inanimate to animate, *Sci. Adv.* 6 (20) (2020) eaba1321.
- [38] C. Huang, J. Dong, W. Sun, Z. Xue, J. Ma, L. Zheng, C. Liu, X. Li, K. Zhou, X. Qiao, Q. Song, W. Ma, L. Zhang, Z. Lin, T. Wang, Coordination mode engineering in stacked-nanosheet metal-organic frameworks to enhance catalytic reactivity and structural robustness, *Nat. Commun.* 10 (1) (2019) 2779.
- [39] M.A. Khalilzadeh, S. Tajik, H. Beitollahi, R.A. Venditti, Green synthesis of magnetic nanocomposite with iron oxide deposited on cellulose nanocrystals with copper ($\text{Fe}_3\text{O}_4/\text{CNC}/\text{Cu}$): investigation of catalytic activity for the development of a venlafaxine electrochemical sensor, *Ind. Eng. Chem. Res.* 59 (10) (2020) 4219–4228.
- [40] Y. Zhang, N. Li, Y. Xiang, D. Wang, P. Zhang, Y. Wang, S. Lu, R. Xu, J. Zhao, A flexible non-enzymatic glucose sensor based on copper nanoparticles anchored on laser-induced graphene, *Carbon N Y* 156 (2020) 506–513.
- [41] L. Fu, A. Wang, K. Xie, J. Zhu, F. Chen, H. Wang, H. Zhang, W. Su, Z. Wang, C. Zhou, S. Ruan, Electrochemical detection of silver ions by using sulfur quantum dots modified gold electrode, *Sens. Actuators B* 304 (2020), 127390.
- [42] S. Hussain, N. Farooq, A.S. Alkorbi, R. Alsaiani, N.A. Alhemiary, M. Wang, Gu. Qiao, Polyhedral $\text{Co}_3\text{O}_4/\text{ZnO}$ nanostructures as proficient photocatalysts for vitiation of organic dyes from waste water, *J. Mol. Liq.* 362 (2022) 119765, <https://doi.org/10.1016/j.molliq.2022.119765>.
- [43] P. Vaid, P. Raizada, A.K. Saini, R.V. Saini, Biogenic silver, gold and copper nanoparticles - a sustainable green chemistry approach for cancer therapy, *Sustain. Chem. Pharm.* 16 (2020), 100247.
- [44] W.-W. Liu, W. Jiang, Y.-C. Liu, W.-J. Niu, M.-C. Liu, K. Zhao, L.-Y. Zhang, L. Lee, L.-B. Kong, Y.-L. Chueh, Platinum-free ternary metallic selenides as nanostructured counter electrode for high-efficiency dye-sensitized solar cell by interface engineering, *ACS Appl. Energy Mater.* 3 (4) (2020) 3704–3713.
- [45] N.A. Khan, N. Rashid, M. Junaid, M.N. Zafar, M. Faheem, I. Ahmad, NiO/NiS heterostructures: an efficient and stable electrocatalyst for oxygen evolution reaction, *ACS Appl. Energy Mater.* 2 (5) (2019) 3587–3594.
- [46] Y. Wang, W. Wei, J. Zeng, X. Liu, X. Zeng, Fabrication of a copper nanoparticle/chitosan/carbon nanotube-modified glassy carbon electrode for electrochemical sensing of hydrogen peroxide and glucose, *Microchim. Acta* 160 (1–2) (2008) 253–260.
- [47] M. Valodkar, S. Modi, A. Pal, S. Thakore, Synthesis and anti-bacterial activity of Cu, Ag and Cu–Ag alloy nanoparticles: a green approach, *Mater. Res. Bull.* 46 (3) (2011) 384–389.
- [48] L.-u. Rahman, A. Shah, S.K. Lunsford, C. Han, M.N. Nadagouda, E. Sahle-Demessie, R. Qureshi, M.S. Khan, H.-B. Kraatz, D.D. Dionysiou, Monitoring of 2-butanone using a Ag–Cu bimetallic alloy nanoscale electrochemical sensor, *RSC Adv.* 5 (55) (2015) 44427–44434.
- [49] C. Minelli, D. Bartzczak, R. Peters, J. Rissler, A. Undas, A. Sikora, E. Sjöström, H. Goenaga-Infante, A.G. Shard, Sticky measurement problem: number concentration of agglomerated nanoparticles, *Langmuir ACS J. Surf. Colloids* 35 (14) (2019) 4927–4935.
- [50] L.U. Rahman, R. Qureshi, M.M. Yasinzi, A. Shah, Synthesis and spectroscopic characterization of Ag–Cu alloy nanoparticles prepared in various ratios, *C.R. Chim.* 15 (6) (2012) 533–538.
- [51] P. Mulvaney, Surface plasmon spectroscopy of nanosized metal particles, *Langmuir* 12 (3) (1996) 788–800.
- [52] A. Pal, S. Shah, S. Devi, Microwave-assisted synthesis of silver nanoparticles using ethanol as a reducing agent, *Mater. Chem. Phys.* 114 (2–3) (2009) 530–532.
- [53] S.H.H. Rahaghi, R. Poursalehi, Optical properties of Ag–Cu alloy nanoparticles synthesized by DC Arc discharge in liquid, *Procedia Mater. Sci.* 11 (2015) 738–742.
- [54] L. Zongquan, S. Hui, C. Li, Characterization of nanocrystalline Ag–Cu alloy, *J. Mater. Res.* 8 (1994) 392–396.
- [55] N. Hikmah, N.F. Idrus, J. Jai, A. Hadi, Synthesis and characterization of silver-copper core-shell nanoparticles using polyol method for antimicrobial agent, *IOP Conf. Ser. Earth Environ. Sci.* 36 (2016), 012050.
- [56] F. Lauraux, T.W. Cornelius, S. Labat, M.I. Richard, S.J. Leake, T. Zhou, O. Kovalenko, E. Rabkin, T.U. Schüllli, O. Thomas, Multi-wavelength Bragg coherent X-ray diffraction imaging of Au particles, *J. Appl. Crystallogr.* 53 (1) (2020) 170–177.
- [57] E. Temur, M. Eryigit, B. Kurt Urhan, Ü. Demir, T. Öznültür Özer, Cu/ Electrochemically reduced graphene oxide layered nanocomposite for non-enzymatic H_2O_2 sensor, *Mater. Today Proc.* 46 (2021) 6971–6975.
- [58] N. Wang, Y. Han, Y. Xu, C. Gao, X. Cao, Detection of H_2O_2 at the nanomolar level by electrode modified with ultrathin AuCu nanowires, *Anal. Chem.* 87 (1) (2015) 457–463.
- [59] M. Merisalu, J. Kruusma, C.E. Banks, Metallic impurity free carbon nanotube paste electrodes, *Electrochem. Commun.* 12 (1) (2010) 144–147.
- [60] J. Kruusma, V. Sammelselg, C.E. Banks, A systematic study of the electrochemical determination of hydrogen peroxide at single-walled carbon nanotube ensemble networks, *Electrochem. Commun.* 10 (12) (2008) 1872–1875.
- [61] D. Li, L. Meng, S. Dang, D. Jiang, W. Shi, Hydrogen peroxide sensing using Cu_2O nanocubes decorated by Ag–Au alloy nanoparticles, *J. Alloy. Compd.* 690 (2017) 1–7.